**Applied Mathematical Sciences, Vol. 1, 2007, no. 19, 939 - 961**

# Fuzzy Classification of Physiographic Features Extracted from Multiscale DEMs

**S. Dinesh**

Science and Technology Research Institute for Defence (STRIDE), D/A KD Malaya
Pangkalan TLDM, 32100 Lumut, Perak, Malaysia
dinsat@yahoo.com

**Abstract**

Geomorphological landforms are generally viewed as Boolean objects. However, recent studies have shown that landforms are more suitable to be viewed as fuzzy objects, whereby a landform is defined as a region in the continuum of variation of the surface of the earth. In this paper, the fuzzy classification of physiographic features extracted from multiscale DEMs is performed. First, the lifting scheme is used to generate multiscale DEMs. The three predominant physiographic features, mountains, basins and piedmont slopes, are extracted from the generated multiscale DEMs. Fuzzy classification is performed based on by the average of Boolean memberships of the extracted physiographic features over the scales of measurement. Using the generated fuzzy memberships, the dominant physiographic features, and their variances, are computed. The proposed fuzzy classification method is useful for statistical analyses and determination of sample schemes.

**Keywords:** multiscale DEMs, physiograhic features, the lifting scheme, fuzzy classification, entropy

## 1 Introduction

In Boolean set theory, if an object belongs to a set, it is assigned an integer value of 1 as membership for that set. If the object does not belong to that set, it is assigned with a membership of 0. In fuzzy set theory, a core concept is defined and objects which exactly match that core concept are assigned with a class membership of 1. The membership is assigned a reducing real number for objects as they are increasingly dissimilar from that core concept until they have no similarity with the core concept, when the membership is assigned a value of 0 [36].

Geomorphological landforms are generally viewed as Boolean objects. However, recent studies have shown that landforms are more suitable to be viewed as fuzzy objects, whereby a landform is defined as a region in the continuum of variation of the surface of the earth [1-3, 11-15, 24, 25, 31, 32]. In general, three approaches have been employed to perform the fuzzy classification of various landforms. The first approach, known as the semantic import model, uses a *priori* knowledge, such as height, to assign a value of fuzzy membership to a landscape feature with a particular metric property [8]. Usery [31] determines the fuzziness of Stone Mountain, Georgia, using the height above a certain elevation as a membership function, with membership increasing with height. Cheng and Molenaar [4, 5] use height to determine membership functions of separate elements of dynamic beach landforms. The second approach, known as the similarity relation model, uses surface derivatives, such as slope and curvature, as input to a multivariate fuzzy classification which yields the membership values [2, 3, 16, 19]. In the third approach, fuzzy classification of landforms is performed based on landforms extracted from multiscale DEMs. In Fisher et al. [14], a multiscale approach to the definition of the fuzzy set membership of morphometric classes of landscape is studied. Using the English Lake District region as a case study, fuzzy classification of the six basic morphometric features (peaks, pits, passes, channels, ridges, planes) are generated.

In this paper, the fuzzy classification of physiographic features extracted from multiscale DEMs is performed. Physiography (also known as land surface characteristics) is the study of the physical features and attributes of the earth's land surface. The

detection of the physiographic features of a terrain is the first phase involved in the classification of the various landforms of the terrain.

In Section 2, the lifting scheme is used to generate multiscale DEMs. In Section 3, the three predominant physiographic features, mountains, basins and piedmont slopes, are extracted from the generated multiscale DEMs using the mathematical morphological based physiographic segmentation algorithm proposed in Dinesh et al. [10]. In Section 4, the fuzzy classification of the extracted physiographic features is performed based on by the average of Boolean memberships of the extracted physiographic features over the scales of measurement. Using the generated fuzzy memberships, the dominant physiographic features, and their variances, are computed. Concluding remarks regarding the scope of the study is provided in the final section.

## 2 Generation of Multiscale DEMs using the Lifting Scheme

Feature detection and characterization often need to be performed at different of scales of measurement. Wood [34, 35] shows that analysis of a region at multiple scales allows for a greater amount of information to be extracted from the DEM about the spatial characteristics of a feature. The term scale refers to combination of both spatial extent and spatial detail or resolution [30]. In this paper, the variation in the spatial extent over which physiographic features are defined is used as the basis to perform fuzzy classification.

In this paper, multiscaling is performed using the lifting scheme [28, 29]. The lifting scheme is a flexible technique that has been used in several different settings, for easy construction and implementation of traditional wavelets and of second generation wavelets, such as spherical wavelets. Lifting consists of the following three basic operations (Figure 1):

### Step 1: Split

The original data set $x[n]$ is divided into two disjoint subsets, even indexed points $x_e[n]=x[2n]$, and odd indexed points $x_0[n]=x[2n+1]$.

**Step 2: Predict**

The wavelet coefficients $d[n]$ are generated as the error in predicting $x_0[n]$ from $x_e[n]$ using the prediction operator P:

$$d[n]=x_0[n\ ]- P(x_e[n]) \quad (1)$$

**Step 3: Update**

Scaling coefficients $c[n]$ that represent a coarse approximation to the signal $x[n]$ are obtained by combining $x_e[n]$ and $d[n]$. This is accomplished by applying an update operator $U$ to the wavelet coefficients and adding to $x_e[n]$:

$$c[n]=x_e[n] + U \quad (2)$$

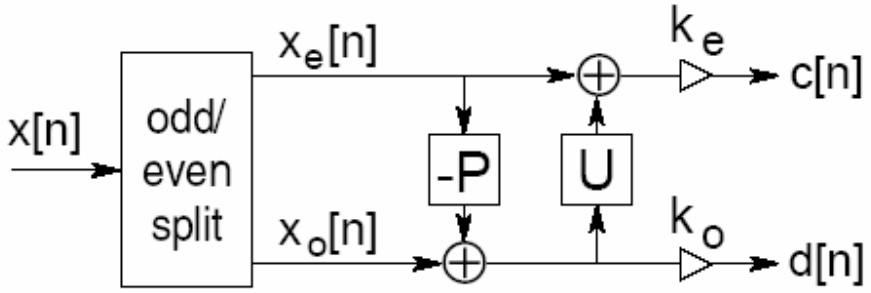


Figure 1: Lifting stage: split, predict, update; $k_e$ and $k_o$ normalize the energy of the underlying scaling and wavelet functions.
(Source: Claypoole and Baraniuk [6])

These three steps form a lifting stage. Using a DEM as the input, an iteration of the lifting stage on the output $c[n]$ creates the complete set of multiscale DEMs $c_j[n]$ and the elevation loss caused by the change of scale $d_j[n]$.

The DEM in Figure 2 shows the area of Great Basin, Nevada, USA. The area is bounded by latitude 38° 15’ to 42° N and longitude 118° 30’ to 115° 30’W. The DEM was rectified and resampled to 925m in both $x$ and $y$ directions. The DEM is a Global Digital Elevation Model (GTOPO30 DEM) and was downloaded from the USGS GTOPO30 website (http://edcwww.cr.usgs.gov/landdaac/gtopo30/gtopo30.html). GTOPO30 DEMs are available at a global scale, providing a digital representation of the

Earth's surface at a 30 arc-seconds sampling interval. The land data used to derive GTOPO30 DEMs are obtained from digital terrain elevation data (DTED), the 1-degree DEM for USA and the digital chart of the world (DCW). The accuracy of GTOPO30 DEMs varies by location according to the source data. The DTED and the 1-degree dataset have a vertical accuracy of $\pm$ 30m while the absolute accuracy of the DCW vector dataset is $\pm$2000m horizontal error and $\pm$650 vertical error [22].

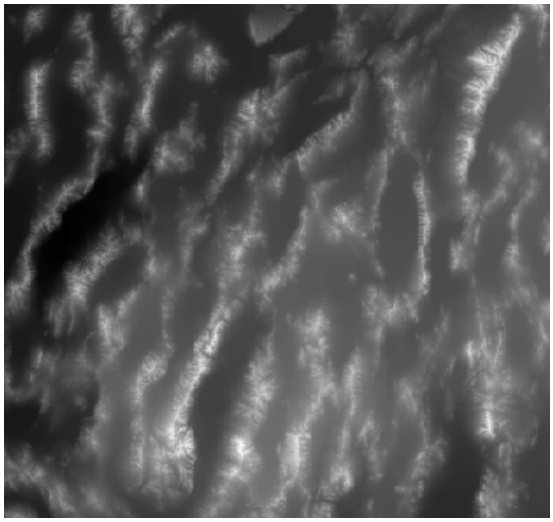

Figure 2: The GTOPO30 DEM of Great Basin. The elevation values of the terrain (minimum 1005 meters and maximum 3651 meters) are rescaled to the interval of 0 to 255 (the brightest pixel has the highest elevation). The scale is approximately 1:3,900,00.

Multiscale DEMs of the Great Basin region are generated by implementing the lifting scheme on the DEM of Great Basin using scales of 1 to 20. As shown in Figure 3, as the scale increases, the merge of small regions into the surrounding grey level regions increases, causing removal of fine detail in the DEM. In Table 1, the generated multiscale DEMs are compared in terms of their:

1) **Mean elevation**: It is computed as the average elevation of the pixels that belong to an object's region. It is interpreted as a measure of the volume of the object per unit area.
2) **Mean gradient**: It is computed as the average value of gradient of pixels constituting an object's region.
3) **Local relief**: The local relief for a finite area of surface was defined as the difference between the maximum elevation and minimum elevation occurring within that area [20].
4) **Relative Massiveness**: Hypsometry studies the distributions of elevations across an area of land from one catchment to the entire planet [7]. The hypsometric integral (HI) is a process indicator reflecting the stage of landscape development [27] and measures the extent to which a land surface has been opened up by erosion [7]. More specifically, areas with HI above 0.6 are in the "youthful" stage, areas with HI between 0.35 and 0.6 are in the "equilibrium or mature" stage and area with HI below 0.35 are in a transitory "monadnock" stage [27]. From a mathematical point of view, HI equals to the relative massiveness, {Mean elevation – minimum elevation} to {Local relief} [23]. The advantage of relative massiveness is that it is easier to compute. Low relative massiveness values occur in terrain characterised by isolated relief features standing above extensive level surfaces, while high values describe broad, somewhat level surfaces broken by occasional depressions [22].

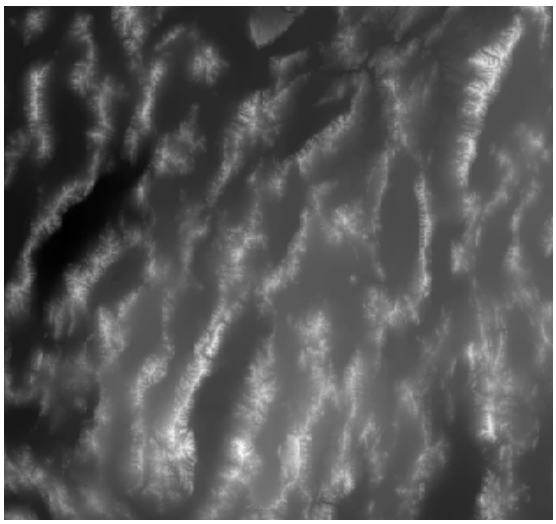

(a)

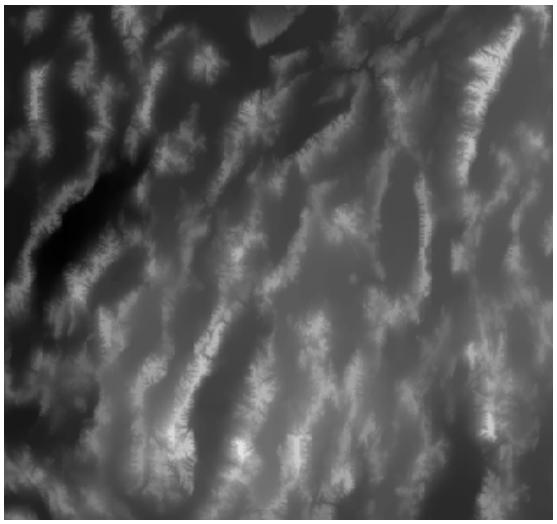

(b)

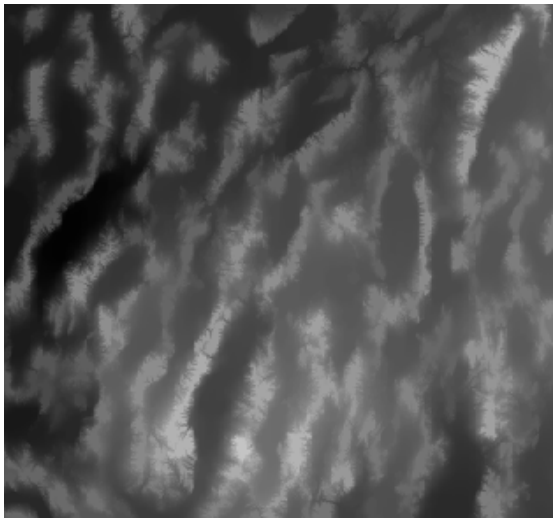

(c)

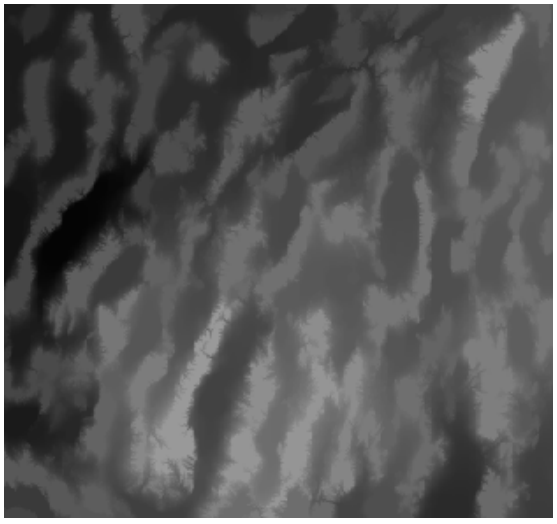

(d)

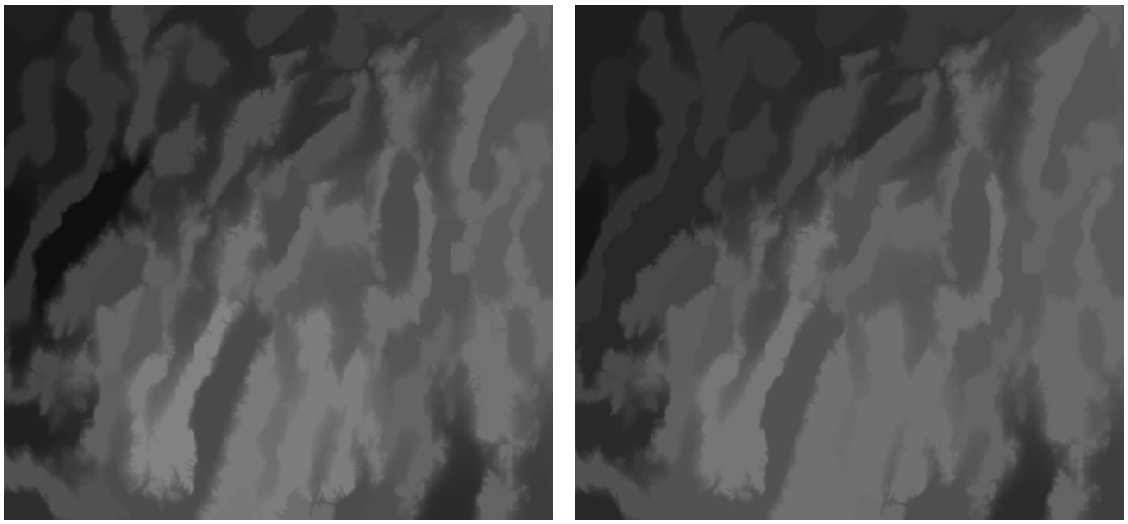

(e) (f)

Figure 3: Multiscale DEMs generated using scales of : (a) 1 (b) 3 (c) 5 (d) 10 (e) 15 (f) 20.

Table 1: Statistics of the generated multiscale DEMs.

| **Scale** | **Maximum elevation (grey level)** | **Mean gradient (°)** | **Local relief** | **Relative massiveness** |
|---|---|---|---|---|
| 1 | 85.13 | 5.94 | 255 | 0.33 |
| 2 | 84.87 | 5.55 | 240 | 0.35 |
| 3 | 84.52 | 5.15 | 227 | 0.37 |
| 4 | 84.06 | 4.77 | 202 | 0.41 |
| 5 | 83.62 | 4.46 | 194 | 0.42 |
| 6 | 83.18 | 4.20 | 183 | 0.44 |
| 7 | 82.72 | 3.93 | 171 | 0.47 |
| 8 | 82.14 | 3.66 | 163 | 0.49 |
| 9 | 81.71 | 3.47 | 163 | 0.48 |
| 10 | 81.06 | 3.20 | 149 | 0.52 |
| 11 | 80.73 | 3.05 | 143 | 0.53 |
| 12 | 80.37 | 2.89 | 135 | 0.54 |
| 13 | 79.54 | 2.60 | 127 | 0.56 |
| 14 | 79.08 | 2.44 | 125 | 0.54 |
| 15 | 78.55 | 2.26 | 115 | 0.55 |
| 16 | 78.09 | 2.10 | 109 | 0.55 |
| 17 | 77.83 | 1.96 | 107 | 0.56 |
| 18 | 77.69 | 1.86 | 106 | 0.56 |
| 19 | 77.51 | 1.75 | 104 | 0.57 |
| 20 | 77.39 | 1.67 | 99 | 0.59 |

## 3 Extraction of Physiographic Features from the Generated Multiscale DEMs

The mountains, basins and piedmont slopes of the generated multiscale DEMs are extracted using the mathematical morphological based physiographic segmentation algorithm proposed in Dinesh et. al [10]. Ultimate erosion is used to extract the peaks and pits of the DEM. Conditional dilation is performed on the peaks and pits of the DEM to obtain the mountain and basin pixels respectively. The pixels that are not classified as mountain pixels or basin pixels are assigned as piedmont slope pixels.

A major problem faced in DEM analysis is the presence of spurious peaks and pits, which are by input data error, interpolation procedures and the limited horizontal and vertical resolution of DEMs. Spurious peaks and pits do not correspond to real landscape features and they cause errors in features extracted from DEMs. Hence, a number of approaches have been employed to perform the removal of spurious peaks and pits from DEMs, including mean smoothing [21], Gaussian blurring [18, 26], Kalman filtering [33], the the á Trous algorithm [17] and morphological smoothing by reconstruction [9]. However, when dealing with multiscale DEMs, spurious peaks and pits are to be treated as artifacts of the DEM, rather than errors. Hence, the removal of problem areas caused by spurious peaks and pits is not performed.

As shown in Figures 4 to 6 and Tables 2 to 4, the merging of small regions into the surrounding grey level regions and removal of fine detail in the DEM cause a reduction in the area of the extracted mountains, and an increase in the area of the extracted basins. In general, the area of the piedmont slopes remains relatively constant.

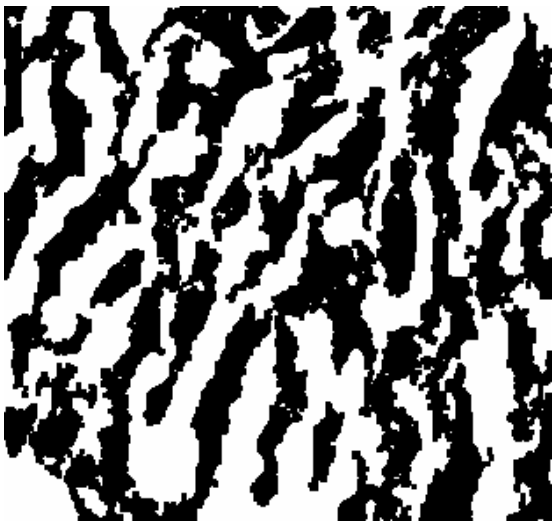

(a)

(b)

(c)

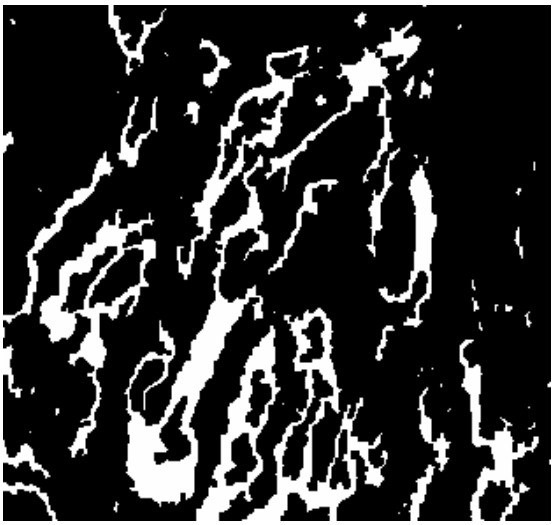

(d)

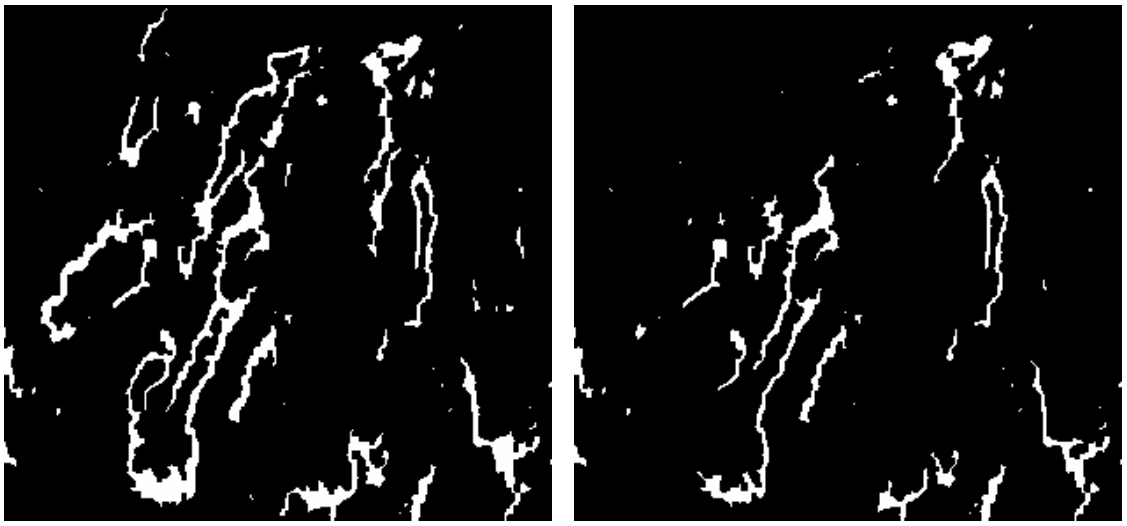

(e) (f)

Figure 4: Mountains (the pixels in white) extracted from the corresponding multiscale DEMs in Figure 2.

Table 2: Statistics of the mountains extracted from the generated multiscale DEMs.

| **Scale** | **Area (pixels)** | **Maximum elevation (grey level)** | **Mean gradient (°)** | **Local relief** | **Relative Massiveness** |
|---|---|---|---|---|---|
| 1 | 44511 | 103.07 | 10.15 | 251 | 0.39 |
| 2 | 41815 | 103.43 | 9.73 | 236 | 0.42 |
| 3 | 40467 | 103.05 | 9.05 | 224 | 0.44 |
| 4 | 37889 | 103.01 | 8.41 | 200 | 0.50 |
| 5 | 34938 | 102.60 | 8.10 | 192 | 0.51 |
| 6 | 32103 | 101.10 | 7.88 | 181 | 0.54 |
| 7 | 28791 | 99.86 | 7.88 | 169 | 0.57 |
| 8 | 26171 | 96.96 | 7.80 | 162 | 0.57 |
| 9 | 21635 | 94.75 | 7.87 | 162 | 0.56 |
| 10 | 16270 | 95.58 | 8.16 | 149 | 0.61 |
| 11 | 15262 | 94.47 | 8.17 | 143 | 0.63 |
| 12 | 13937 | 93.39 | 8.09 | 135 | 0.64 |
| 13 | 11269 | 88.91 | 7.92 | 127 | 0.63 |
| 14 | 9028 | 89.54 | 7.88 | 125 | 0.63 |
| 15 | 7682 | 88.22 | 7.86 | 115 | 0.64 |
| 16 | 6988 | 88.19 | 7.84 | 108 | 0.64 |
| 17 | 6466 | 88.06 | 7.77 | 101 | 0.63 |
| 18 | 5659 | 89.84 | 7.77 | 95 | 0.64 |
| 19 | 4531 | 91.70 | 7.69 | 88 | 0.66 |
| 20 | 4325 | 90.93 | 7.58 | 84 | 0.68 |

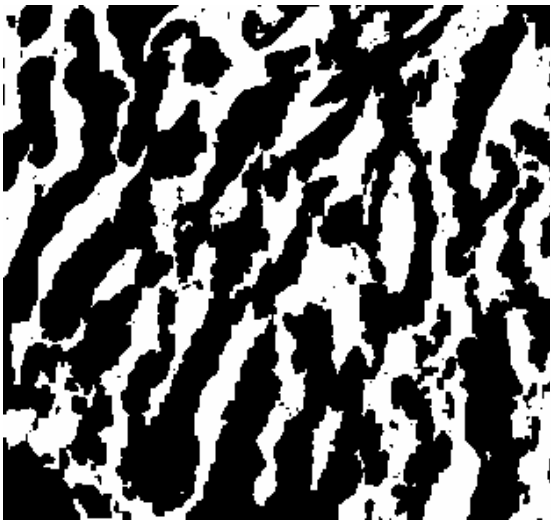

(a)

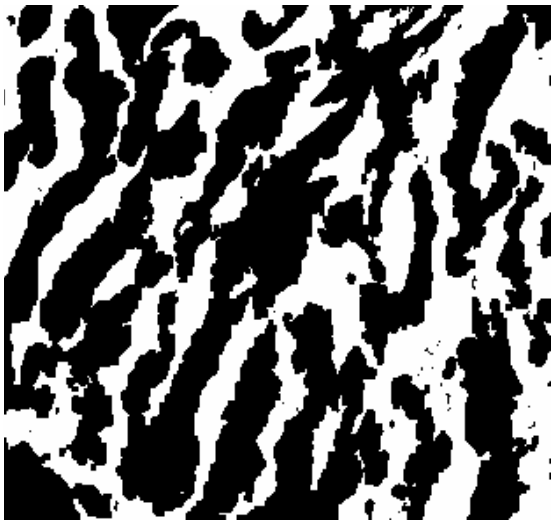

(b)

(c)

(d)

(e) (f)

Figure 5: Basins (the pixels in white) extracted from the corresponding multiscale DEMs in Figure 2.

Table 3: Statistics of the basins extracted from the generated multiscale DEMs.

| Scale | Area (pixels) | Maximum elevation (grey level) | Mean gradient (°) | Local relief | Relative massiveness |
|---|---|---|---|---|---|
| 1 | 36375 | 66.18 | 1.31 | 131 | 0.51 |
| 2 | 37255 | 66.90 | 1.39 | 131 | 0.51 |
| 3 | 38029 | 67.33 | 1.41 | 130 | 0.51 |
| 4 | 38804 | 67.90 | 1.42 | 129 | 0.51 |
| 5 | 39841 | 68.73 | 1.44 | 129 | 0.52 |
| 6 | 41222 | 69.76 | 1.43 | 139 | 0.49 |
| 7 | 43324 | 71.53 | 1.44 | 164 | 0.42 |
| 8 | 45776 | 73.52 | 1.44 | 137 | 0.51 |
| 9 | 48729 | 74.75 | 1.42 | 137 | 0.52 |
| 10 | 51861 | 76.07 | 1.43 | 145 | 0.50 |
| 11 | 55453 | 77.02 | 1.36 | 143 | 0.50 |
| 12 | 55387 | 75.49 | 1.35 | 135 | 0.51 |
| 13 | 58790 | 77.16 | 1.33 | 127 | 0.54 |
| 14 | 65674 | 78.85 | 1.30 | 125 | 0.54 |
| 15 | 70356 | 76.37 | 1.36 | 110 | 0.56 |
| 16 | 73360 | 76.77 | 1.26 | 109 | 0.54 |
| 17 | 69079 | 80.20 | 1.15 | 101 | 0.56 |
| 18 | 70584 | 80.16 | 1.12 | 96 | 0.54 |
| 19 | 72870 | 79.80 | 1.08 | 94 | 0.55 |
| 20 | 73704 | 79.69 | 1.05 | 90 | 0.57 |

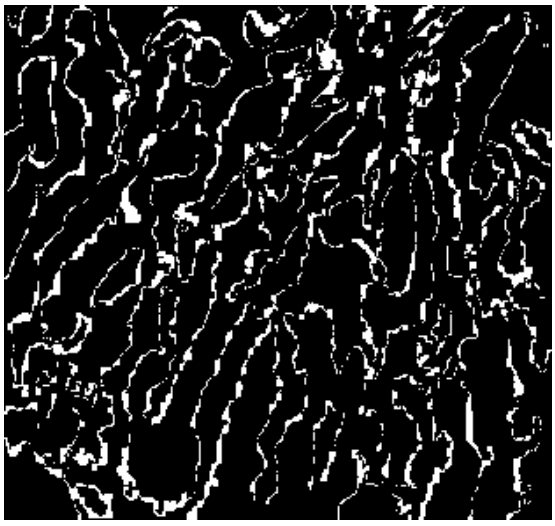

(a)

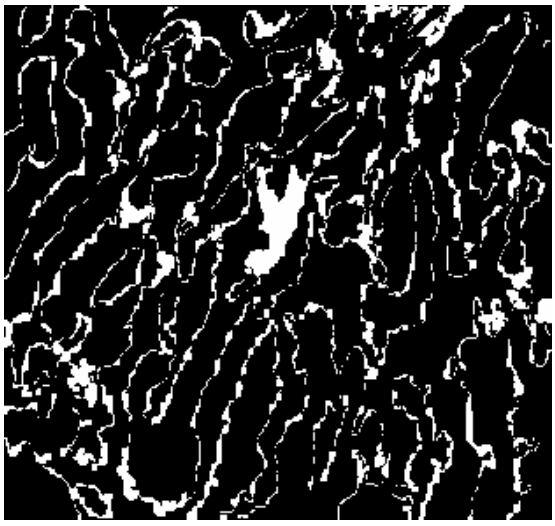

(b)

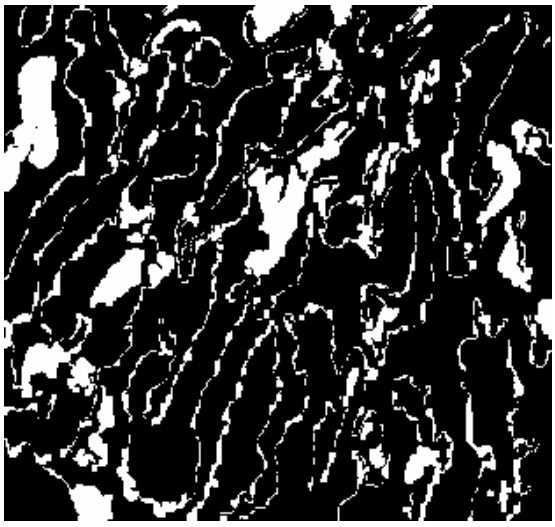

(c)

(d)

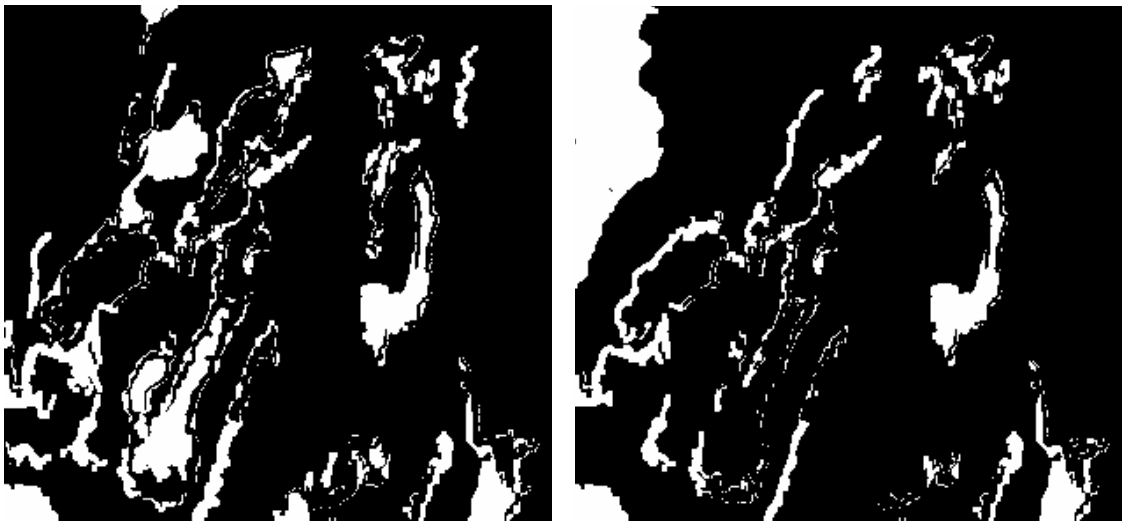

(e) (f)

Figure 6: Piedmont (the pixels in white) extracted from the corresponding multiscale DEMs in Figure 2.

Table 4: Statistics of the piedmont slopes extracted from the generated multiscale DEMs.

| **Scale** | **Area (pixels)** | **Maximum elevation (grey level)** | **Mean gradient (°)** | **Local relief** | **Relative massiveness** |
|---|---|---|---|---|---|
| 1 | 10530 | 74.74 | 4.12 | 135 | 0.54 |
| 2 | 12346 | 76.24 | 3.96 | 140 | 0.53 |
| 3 | 12920 | 77.05 | 3.97 | 140 | 0.54 |
| 4 | 14723 | 77.90 | 4.25 | 140 | 0.54 |
| 5 | 16637 | 79.44 | 4.05 | 149 | 0.52 |
| 6 | 18091 | 81.98 | 3.97 | 142 | 0.56 |
| 7 | 19301 | 82.28 | 3.65 | 164 | 0.49 |
| 8 | 19469 | 82.50 | 3.34 | 154 | 0.52 |
| 9 | 21052 | 84.41 | 3.69 | 157 | 0.52 |
| 10 | 23285 | 82.03 | 3.66 | 149 | 0.52 |
| 11 | 20701 | 80.55 | 3.80 | 143 | 0.53 |
| 12 | 22092 | 84.38 | 3.47 | 135 | 0.57 |
| 13 | 21357 | 81.15 | 3.30 | 127 | 0.57 |
| 14 | 16714 | 74.31 | 3.98 | 125 | 0.51 |
| 15 | 13378 | 84.50 | 3.78 | 115 | 0.60 |
| 16 | 11068 | 80.41 | 4.07 | 108 | 0.57 |
| 17 | 15871 | 63.31 | 3.09 | 107 | 0.42 |
| 18 | 15173 | 61.68 | 3.11 | 106 | 0.41 |
| 19 | 14015 | 61.03 | 3.34 | 104 | 0.41 |
| 20 | 13387 | 60.33 | 3.20 | 99 | 0.42 |

## 4 Fuzzy Classification of the Extracted Physiographic Features

In order to perform the fuzzy classification of the extracted physiographic features, it is first assumed that at any particular scale, each physiographic feature is a Boolean object. Hence, the landform *L*, at location *x*, can be belong the set *[P]* of three possible physiographic features:

$$L_x = [P] \tag{3}$$

Of the 3 valuations of *P*, only one value will have a Boolean membership of 1, while the remaining two will have Boolean memberships of 0. The main reason why physiographic features are more suitable to be considered as fuzzy objects is that the assignment of any location to a physiographic feature is not necessary stable under repeated observation at different scales. Thus, if $m_{P_{x|S_1}} = 1$ for a particular landscape, it does not follow that either $m_{P_{x|S_2}} = 1$, or $m_{P_{x|S_3}} = 1$, where $m_{P_x}$ indicates the membership value at location *x* and $s_1$, $s_2$ and $s_3$ indicate different scales of measurement.

The fuzzy membership of a physiographic feature $\mu_P$ at location *x* can be given by the average of Boolean memberships of that feature over the scales of measurement:

$$\mu_{P_x} = \frac{\sum_{i=1}^{20} m_{P_x|s_i}}{20} \tag{4}$$

Figure 7 shows the fuzzy memberships of the extracted physiographic features. The distribution of the pixels based on their memberships is shown in Table 5.

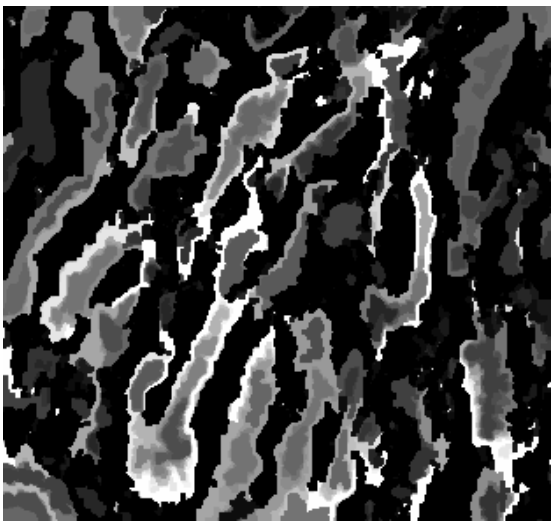

(a)

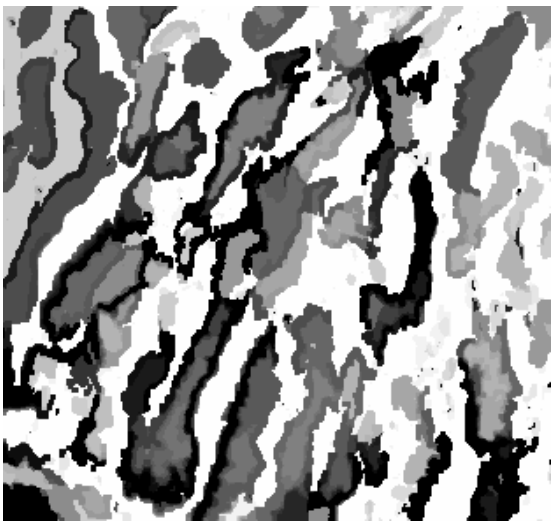

(b)

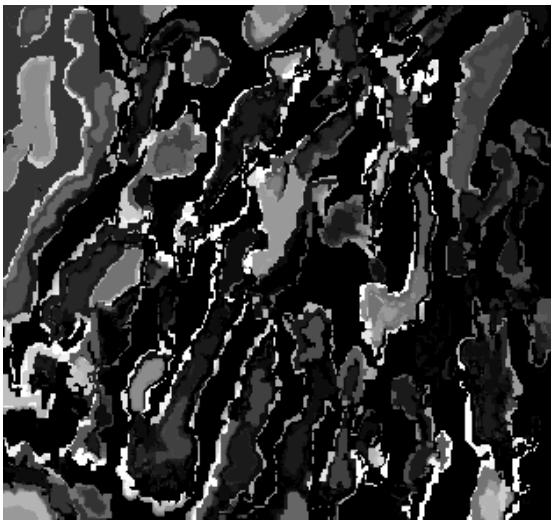

(c)

Figure 7: Fuzzy memberships of the three physiographic features: (a) mountains (b) basins (c) piedmont slopes. The membership values (ranging from 0 to 1) are rescaled to the interval of 0 to 255 (the brightest pixel has the highest membership value).

Table 5: Distribution of the pixels based on their fuzzy memberships.

| **Membership range** | **Mountains (pixels)** | **Basins (pixels)** | **Piedmont Slopes (pixels)** |
|---|---|---|---|
| 0.0-0.1 | 49601 | 12212 | 51744 |
| 0.1-0.2 | 3926 | 4642 | 8691 |
| 0.2-0.3 | 9098 | 10192 | 11559 |
| 0.3-0.4 | 2620 | 5877 | 2188 |
| 0.4-0.5 | 9872 | 5841 | 3709 |
| 0.5-0.6 | 2356 | 4579 | 2396 |
| 0.6-0.7 | 4949 | 4992 | 3242 |
| 0.7-0.8 | 2006 | 3596 | 2659 |
| 0.8-0.9 | 1331 | 5006 | 1246 |
| 0.9-1.0 | 1334 | 2346 | 1464 |

Using the generated fuzzy memberships, the dominant physiographic feature *mod* $P_x$ at location $x$ is defined as:

$$mod\ P_x = max_{j=1}^{3}(\mu_{P_{jx}}) \tag{5}$$

The computed dominant physiographic features are shown in Figure 8. A total of 23,698 pixels (25.92%) are classified as mountains pixels, 53,698 (58.74%) as basin pixels and 14,020 pixels (15.34%) as piedmont slope pixels.

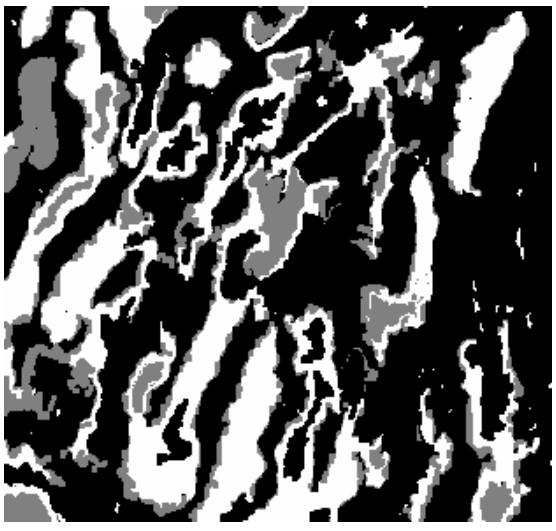

Figure 8: The dominant physiographic features. The mountains pixels are the pixels in white, the piedmont pixels are the pixels in grey and the basin pixels are the pixels in black.

The variance of the computed dominant physiographic features is measured by the entropy $E_x$, which is scaled between 0 (classification agreement at all scales) and 1 (observations split equally between all three features), by dividing the maximum entropy generated by the three physiographic features:

$$E_x = \frac{\sum_{j=1}^{3} \mu_{P_{jx}} \log(\mu_{P_{jx}})}{\log(1/3)} \quad (6)$$

The computed entropy values are shown in Figure 9. The distribution of the pixels based on their entropy values is shown in Table 6.

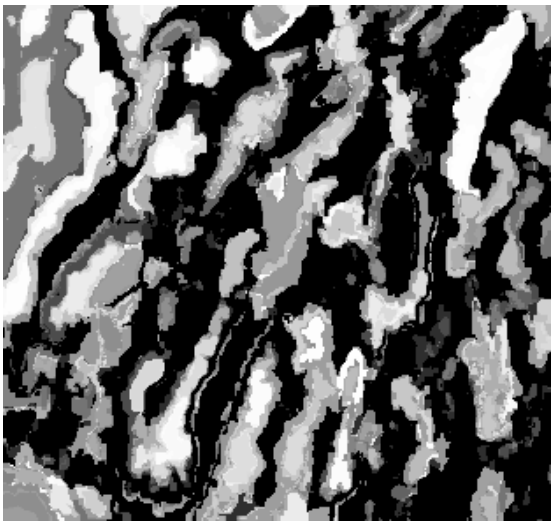

Figure 9: The computed entropy values. The entropy values (ranging from 0 to 1) are rescaled to the interval of 0 to 255 (the brightest pixel has the highest entropy value).

Table 6: Distribution of the pixels based on their entropies.

| Entropy range | Number of pixels |
|---|---|
| 0.0-0.1 | 49601 |
| 0.1-0.2 | 3926 |
| 0.2-0.3 | 9098 |
| 0.3-0.4 | 2620 |
| 0.4-0.5 | 9872 |
| 0.5-0.6 | 2356 |
| 0.6-0.7 | 4949 |
| 0.7-0.8 | 2006 |
| 0.8-0.9 | 1331 |
| 0.9-1.0 | 1334 |

## 4 Conclusion

The fuzzy classification of physiographic features extracted from DEMs was also performed. First, the lifting scheme algorithm was used to generate multiscale DEMs. The three predominant physiographic features, mountains, basins and piedmont slopes, were extracted from the generated multiscale DEMs. Fuzzy classification is performed based on the physiographic features extracted from the multiscale DEMs. Using the generated fuzzy memberships, the dominant physiographic features, and their variance, are computed. The proposed fuzzy classification method is useful for statistical analyses and determination of sample schemes.

## References

1) Burrough, P.A. and Heuvelink, G.B.M., The sensitivity of Boolean and continuous (fuzzy) logical modelling to uncertain data. Proceedings, EGIS 92, Munich 2 (1992), 1032-1041.
2) Burrough, P. A., van Gaans, P. F. M. and MacMillan, R. A., High-resolution landform classification using fuzzy k-means, Fuzzy Sets and Systems, 113(1) (2000), 37-52.
3) Burrough, P. A., Wilson, J.P., van Gaas, P.F.M and Hansen, A.J., Fuzzy k-means classification of topo-climatic data as an aid to forest mapping in the Greater Yellowstone Area, USA. Landscape Ecology, 16 (2001), 523-546
4) Cheng, T. and Molenaar, M., Objects with fuzzy spatial extent. Photogrammetric Engineering and Remote Sensing, 63 (1999a), 403-414.
5) Cheng, T. and Molenaar, M., Diachronic analysis of fuzzy objects. Geoinformatica, 3 (1999b), 337-356.
6) Claypoole, R.L. and Baraniuk, R.G., A multiresolution wedgelet transform for image processing. In M. A. Unser, A. Aldroubi, and Laine A. F., (Eds.) Wavelet Applications in Signal and Image Processing VIII, Volume 4119 of SPIE Proceedings, (2000) 253-262.

7) Cogley, J.G., Hypsometry of the continents. Zeitschrift fiir Geomorphologie. Supplementband, 53 (1985), 1-45.
8) Dehn, M, Gärtner, H. amd Dikau, R., Principles of semantic modeling of landform structures. Computers & Geosciences, 27(8) (2001), 1005-1010.
9) Dinesh, S., Digital elevation smoothening using morphological smoothening by reconstruction. International Conference on Science and Technology: Applications in Industry and Education, 8-9 December 2006, University Teknologi MARA, Pulau Pinang, Malaysia (2006).
10) Dinesh, S., Radhakrishnan, P. and Sagar, B.S.D., Morphological segmentation of physiographic features from DEM. International Journal of Remote Sensing, In press (2007).
11) Fisher, P., Fuzzy modeling. In Openshaw S., Abrahart, R. and Harris, T., eds. Geocomputing, London: Taylor and Francis (2000).
12) Fisher, P., Sorites paradox and vague geographies. Fuzzy Sets and Systems, 113 (2000), 7-18.
13) Fisher, P. and Wood, J., What is a mountain? Or the Englishman who went up a Boolean geographical concept but realised it was fuzzy, Geography, 83(3) (1998), 247-256.
14) Fisher, P., Wood, J. and Cheng, T., Where is Helvellyn? Fuzziness of multiscale landscape morphometry. Transactions of the Institute of British Geographers, 29(1) (2004), 106-128.
15) Gale, S., Inexactness fuzzy sets and the foundation of bahevioral geography. Geographical Analysis, 4 (1972), 337-349.
16) Irvin, B.J., Ventura, S.J. and Slater, B.K., Fuzzy and isodata classification of landform elements from digital terrain data in Pleasant Valley, Wisconsin, Geoderma, 77 (1997), 137-154.

17) John, C.T., Ping, W., Yi, L., Zhijun, W. and Cheng, E.D., Aspects of digital elevation model determination. Symposium on Geospatial Theory, Processing and Applications, Ottawa (2004).

18) Lee, J., Snyder, P.K. and Fisher, P.F., Modelling the effect of data errors on feature extraction from digital elevation models. Photogrammetric Engineering & Remote Sensing, 58 (10) (1992), 1461 -1467.

19) MacMillan, R.A, Pettapiece, W.W., Nolan, S.C. and Goddard, T.W., A generic procedure for automatically segmenting landforms into landform elements using DEMs, heuristic rules and fuzzy logics. Fuzzy Sets and Systems, 113 (2000), 81-109.

20) Mark, D.M., Geomorphometric parameters: A review and evaluation. Geographiska Annaler, 57A (1975), 1461-1467.

21) Mark, D. M., Automatic detection of drainage networks from digital elevation models. Cartographica, 21 (1984), 168-178.

22) Miliaresis, G.C., and Argialas, D.P., Quantitative representation of mountain objects extracted from the Global Digital Elevation Model (GTOPO30). International Journal of Remote Sensing, 23 (5) (2002), 949-964.

23) Pike, R.J. and Wilson, S.E., Elevation-relief ratio, hypsometric integral and geomorphic area-altitude analysis. Geological Society of America Bulletin, 82 (1971), 1079-1084.

24) Robinson, V.B., Some implications of fuzzy set theory applied to geographic databases, Computers, Environment and Urban Systems, 12 (1988), 89-97.

25) Robinson, V.B., A perspective on the fundamentals of fuzzy sets and their use in geographical information systems. Transactions in GIS, 7 (2003), 3-30.

26) Seemuller, W.W., The extraction of ordered vector drainage networks from elevation data. Computer Vision, Graphics and Image Processing, 47 (1989), 45-48.

27) Strahler, A.N., Hypsometric (area-altitude) analysis of erosional topography. Geological Society of America Bulletin, 63 (1952), 1117-1142.

28) Sweldens, W., 1996. The lifting scheme: A custom-design construction of biothorgonal wavelets. Applied Computational Harmonics and Analysis, 3(2), 186-200.

29) Sweldens, W., 1997. The lifting scheme: A construction of second generation wavelets. Journal of Mathematical Analysis, 29(2), 511-546.

30) Tate, N. and Wood, J., Fractals and scale dependencies in topography. In Tate, N. and Atkinson, P. (Eds.). Modelling Scale in Geographical Information Science. Wiley, Chicester (2001), 35-51.

31) Usery, E.L., A conceptual framework and fuzzy set implementation for geographic features, in Burrough, P. A. and Frank, A. (Eds.) Geographic objects with indeterminate boundaries. London: Taylor and Francis (1996), 87-94.

32) Varzi, A.C. Vagueness in geography. Philosophy and Geography, 4 (2001), 49-65.

33) Wang, P., Applying two dimensional Kalman filtering on digital elevation models. Photogrammetric Engineering & Remote Sensing, 32(4) (1998), 649-656.

34) Wood, J., Scale-based characterization of digital elevation models. In Parker, D. (Eds.) Innovation in GIS 3. Taylor & Francis, London (1996), 163-175.

35) Wood, J., The Geomorphological Characterization of Digital Elevation Models, PhD Thesis, Department of Geography, University of Leicester, Leicester (1996).

36) Zadeh, L.A, Fuzzy sets. Information and Control, 8 (1965), 338-353.

**Received: January 4, 2007**